Finite element simulations of a hip joint with femoroacetabular impingement

J.P. Jorge, F.M.F. Simões, E.B. Pires, P.A. Rego, D.G. Tavares, D.S. Lopes & A. Gaspar

Taylor & Francis
Taylor & Francis Group

Finite element simulations of a hip joint with femoroacetabular impingement

J.P. Jorge[a], F.M.F. Simões[b,c]*, E.B. Pires[b], P.A. Rego[d], D.G. Tavares[b], D.S. Lopes[e] and A. Gaspar[f]

[a]ISR, Instituto Superior Técnico, Technical University of Lisbon, Avenida Rovisco Pais, 1049-001 Lisbon, Portugal; [b]ICIST, Instituto Superior Técnico, Technical University of Lisbon, Avenida Rovisco Pais, 1049-001 Lisbon, Portugal; [c]Department of Civil Engineering and Architecture, Instituto Superior Técnico, Technical University of Lisbon, Avenida Rovisco Pais, 1049-001 Lisbon, Portugal; [d]Clínica Universitária de Ortopedia, Medical School, University of Lisbon, Avenida Professor Egas Moniz, 1649-028 Lisbon, Portugal; [e]IDMEC, Instituto Superior Técnico, Technical University of Lisbon, Avenida Rovisco Pais, 1049-001 Lisbon, Portugal; [f]Department of Imagiology, Hospital da Luz, Avenida Lusíada, 100, 1500-650 Lisbon, Portugal

In this study, a three-dimensional finite element (FE) model based on the specific anatomy of a patient presenting a femoroacetabular impingement of the 'cam'-type is developed. The FE meshes of the structures of interest are obtained from arthrographic magnetic resonance images. All soft tissues are considered linear elastic and isotropic, and the bones were assumed rigid. A compression of the femur on the acetabular cavity as well as flexural movements and internal rotations are applied. Stresses and contact pressures are evaluated in this patient-specific model in order to better interpret the mechanism of aggression of the femoral and acetabular cartilages. The corresponding results are presented and discussed. The values obtained for the contact pressures are similar to those reported by other models based on idealised geometries. An FE analysis of a non-cam hip is also performed for comparison with the pathological case.

Keywords: hip joint; impingement; finite elements; geometric modelling; contact pressures

1. Introduction

The hip joint plays a fundamental role in human locomotion. It is a ball-and-socket joint whose articular cartilage is submitted to contact stresses for any rotations of the femoral head in the gait cycle. Hip joint degeneration remains a common cause of disability often leading to surgical replacement with prosthetic devices. The femoroacetabular impingement (FAI) depends on an abnormal morphological relation between the femoral head and the acetabular cavity. The 'cam'-type FAI is due to the presence of a non-spherical portion of the femoral head usually located at the antero-superior quadrant of the region of transition with the anatomical neck. This impingement was first described by Ganz et al. (2003) as a potential cause for human osteoarthritis (OA) (Wagner et al. 2003; Leunig et al. 2006). The proposed mechanism consists of a chronic abnormal compression on the peripheral acetabular cartilage caused by the non-spherical portion of the femoral head that penetrates into the socket. Due to this asphericity, the peripheral acetabular cartilage is submitted to a non-physiological excessive pressure during flexural movements and/or internal rotations that can cause macroscopic visible lesions (Wagner et al. 2003; Beck et al. 2004). These lesions seem to be similar, from the pathological and biochemical points of view, to those existing in advanced OA (Wagner et al. 2003). In some cases, an increasing gradient of these lesions from the equator of the head to the periphery where the radius of curvature is larger can be observed. This abnormal compression may occur in sport or in some cases even in daily activities. The treatment for this deformity is essentially surgery (Clohisy and McClure 2005) and relies on trimming the head-neck junction to remove the non-spherical part of the head (osteochondroplasty).

In the last decade, the cam-type FAI has received a growing attention, namely in what concerns the description of the mechanism of lesion of the articular cartilage and its possible relation with OA. Several experimental (Hodge et al. 1986; Afoke et al. 1987; Macirowski et al. 1994; Michaeli et al. 1997; von Eisenhart et al. 1999; Anderson et al. 2008) and computational (Macirowski et al. 1994; Genda et al. 2001; Bachtar et al. 2006; Yoshida et al. 2006; Anderson et al. 2008) studies have been performed in order to evaluate the contact pressures in the hip joint and to correlate the morphological anomaly with the intra-articular contact pressure developed in routine activities. Recently Chegini et al. (2009) used the finite element (FE) method to evaluate the contact pressures in virtual models of hips with FAI of the type 'cam' and/or 'pincer' and of hips with dysplasia. To our knowledge, there are no computational studies based on the reconstruction of the real deformity of patients characterising the pressures in the contact between the non-spherical portion of the femoral head and the acetabulum as a result of the movements involved in the joint.

---

*Corresponding author. Email: fsimoes@civil.ist.utl.pt

The objective of this study is to evaluate the order of magnitude of the pressures at the contact zone of the femoral head as well as the stresses in the cartilages as a result of the abnormal contact between the different tissues in a patient presenting a cam-type deformity. Preliminary results can be found in Jorge et al. (2010). Comparisons with a non-cam hip and with models obtained from idealised geometries, as well as with clinical and intra-operative observations, are also intended. This subject-specific three-dimensional (3D) model may contribute to a better understanding of the mechanism of aggression of the femoral and acetabular cartilages.

2. Methods

For the radiological study of certain pathologies of the hip joint, the acquisition of a set of radial images with a common axis positioned along the femoral neck and containing the centre of rotation of the femoral head is usually preferred because it allows medical doctors to visualise the anatomical set. In this study, a 3D reconstruction methodology (Lopes et al. 2010) is applied to a hip joint of a 27-year-old male with a cam-type deformity. The deformity is located at the right hip with an alpha angle of 98° (normal value up to 40°) and a Wiberg's centre-edge (CE) angle of 30° (value considered normal). Figure 1(a) shows 16 images of the hip joint which were radially acquired with a rotation axis coincident with the geometric axis of the femoral neck. The distinguishing anatomical structures are the following: the head and anatomical neck of the femur, the femoral and acetabular cartilages, the acetabulum and the labrum. The radial magnetic resonance arthrography (MRA) T2 signal images are acquired from a Siemens® MAGNETOM Avanto 1.5T (repetition time (ms)/echo time (ms), 852/22; field of view, 21 cm; matrix, 512×512; x and y pixel

resolution, 0.4102 mm; section thickness, 3 mm; number of signals acquired, two) after an injection of an intra-articular 9% saline solution with gadolinium. Further image processing, e.g. contrast enhancement and anthropometric measures, is performed with the software OsiriX v.3.1. The radial angles of acquisition vary from 0° to 168.75°, with angular increments of 11.25°.

The software tools needed to obtain the 3D model incorporate several algorithm blocks, each with specific functionalities in the overall modelling scheme: image segmentation, point cloud interpolation, mesh generation and adjustment, and solid model construction. Using Rhinoceros®, the 16 MRA images are manually segmented with spline curves in order to extract the geometrical data relative to the contours that delimit the anatomical structures of interest (Figure 1(b)), and from these contours a cloud of points is extracted. For the 3D reconstruction of the hip joint, a mathematical surface representation based on the geometrical data extracted from the images (Figure 1(a)) must be determined. For this purpose, an implicit surface interpolation technique based on radial basis functions (RBFs) is considered. Several works have already demonstrated the effectiveness of RBF applied to medical data (Carr et al. 1997, 2001; Teodoro et al. 2009). This method allows the interpolation and extrapolation of a cloud of points in order to obtain an implicit representation of the surface (FarField Technology – FastRBF interpolation toolboxes designed for MATLAB®). Reconstructions of the surfaces of all the structures obtained following the above-mentioned methodology can be found in Lopes et al. (2010). 3D solid models of the cartilages and labrum are then generated using SolidWorks®, in which the triangular surfaces are interpolated with B-spline cubic patches. Manual segmentation and the 3D reconstruction were performed under the supervision of a senior orthopaedic surgeon.

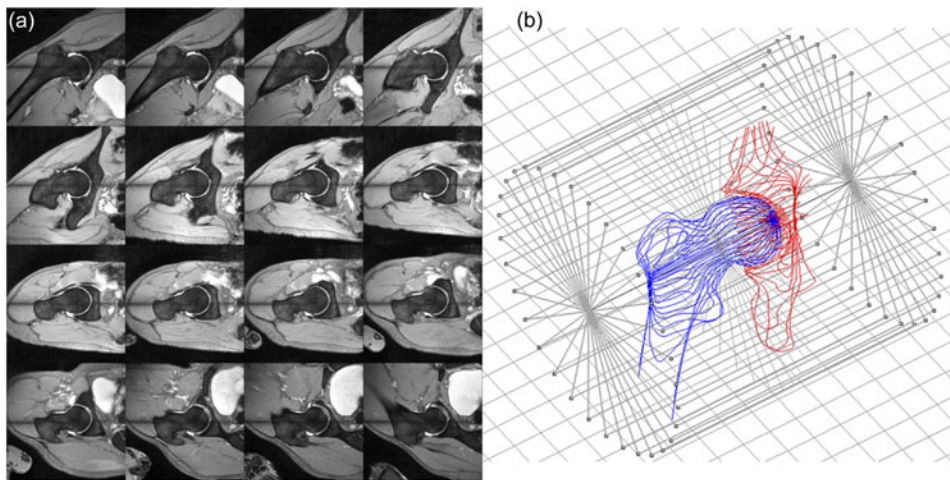Figure 1. (a) Set of 16 radial MRA images (top left image corresponds to 0°, the bottom right image to 168.75°, for the in-between images the angle varies row-wise); (b) the 16 acquisition planes and their position relative to the femur and acetabulum.

Previous 2D analyses considering the bony structures to be linear elastic and rigid showed practically the same values for the maximum pressure at the contact between the two cartilages (Lopes et al. 2009). Therefore, all the present analyses are performed considering the femur and the acetabulum as rigid. The solid models are automatically discretised into FEs using Abaqus CAE® v.6.8. Figure 2 shows the complete FE mesh of the cartilaginous tissues with a total of 109,167 tetrahedral elements. A study on the convergence of the mesh provided a similar value for the maximum contact pressure at the same node before application of the rotational movements when linear and quadratic elements are used (5.2 and 5.1 MPa, respectively). Therefore, the subsequent rotational movements are performed only with the mesh of linear elements. The cartilages and the labrum are considered linear elastic and isotropic with $E = 12$ MPa for the former (Shepherd and Seedhom 1997) and $E = 20$ MPa for the latter (Chegini et al. 2009). For both soft tissues, Poisson's ratio has a value of 0.4. The outer surfaces of the soft tissues in contact with the acetabulum are fixed. All the analyses performed with Abaqus® v.6.8 are geometrically non-linear. A surface-to-surface contact is adopted between the femoral cartilage, as master surface, and the acetabular cartilage and labrum (considered to be tied together), as slave surfaces. The interaction between these two surfaces is considered frictionless and the parameter 'finite sliding' is used. First, the hip joint is subjected only to a compression force applied at the centroid of the femoral head. This force acts in the frontal plane with a component of 480 N along the horizontal axis (x-axis) and a component of 2000 N along the vertical axis (y-axis). These values correspond to the maximum force observed in a routine activity (walking) and for 800 N individual weight (Bergmann et al. 2001) (Figure 2). With the joint subjected to the compression force, several movements within the physiological range are simulated: a flexural rotation of the femur (about the
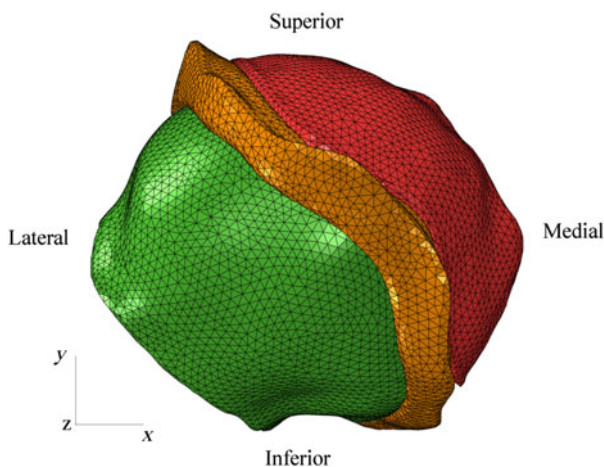
x-axis) of 90°, a pure internal rotation (about the y-axis) of 24° and combined movements of flexural followed by internal rotations. In the pure flexural and internal rotations, four nodes in the FE mesh of the femoral cartilage are selected, defining straight lines perpendicular to the axis of rotation (Figure 3(a),(b)). The extremities of these lines are located in the highest and lowest (transition to the cephalic region closest to the neck in the case of the pure flexion or equatorial region in the case of the pure internal rotation) regions of the cam deformity. The contact pressure is registered in each one of these nodes as a function of the angular movement of the femoral head. Distributions of the contact pressures in the acetabular and femoral cartilages, their maximum values and the von Mises stresses (related to the distortional strain energy) are also presented at the end of both rotations.

An FE analysis of a non-cam hip is also performed for comparison with the pathological case. The same 3D reconstruction methodology is applied to the non-cam hip joint (alpha angle of 48°) of a 50-year-old female. Figure 4 shows the complete FE mesh of the cartilaginous tissues with a total of 181,880 tetrahedral linear elements. The mechanical properties of the tissues of the non-cam hip model are equal to those of the cam hip model, and both models are subjected to the same boundary and loading conditions. As in the cam hip model, four nodes in the FE mesh of the femoral cartilage are selected defining straight lines perpendicular to the axis of flexural rotation and to the axis of internal rotation (Figure 5(a),(b)), and the contact pressure is registered in each one of these nodes as a function of the angular movement of the femoral head. These nodes are located in regions corresponding to the ones to which the nodes selected in the deformity of the cam hip belong.

3. Results

In Table 1, the maximum values for the amplitude of the different movements in the patient before the surgery, those obtained with the model and the maximum contact pressures are presented. At the end of the pure (isolated) flexural movement and of the 90° flexion followed by an internal rotation, the patient felt pain. In the case of the 30° flexion followed by internal rotation, the patient presented a mechanical limitation without pain. The maximum clinical angular displacements of the right hip of the selected patient (measured with a goniometer) are comparable with the maximum possible amplitudes obtained with the model. In fact the FE analysis of the pure flexion case reached 90°, but in the other three cases (90° flexion and internal rotation, 30° flexion and internal rotation and pure internal rotation) they stopped at the indicated values (2.8°, 12.8° and 24° of internal rotation, respectively) due to lack of convergence.

The transarticular compression led to a progressive increase in the contact pressure in the load area of the joint.

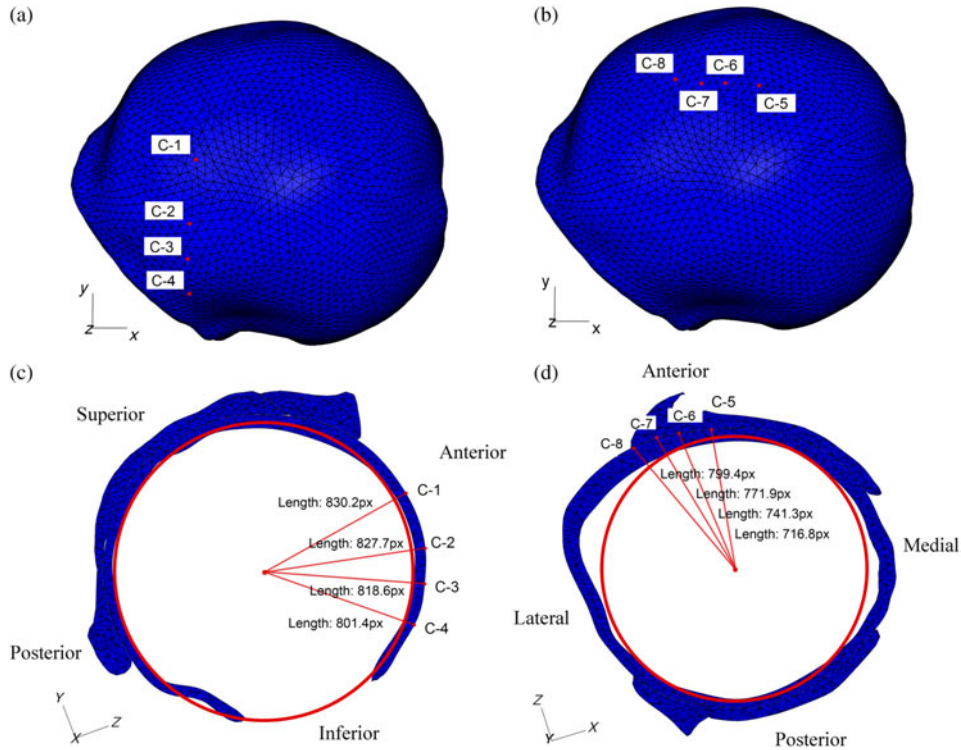Figure 2. FE mesh of the complete model.

Figure 3. FE mesh of the femoral cartilage with the chosen surface nodes for (a) the pure flexion and (b) the pure internal rotation. The distance of the selected nodes to the axis of rotation (c) decreases in the direction of the femoral neck and (d) increases in the direction of the equator of the femoral head.

The maximum contact pressure before application of the rotational movements occurs at a node located in the antero-internal region with a value of 5.2 MPa. A maximum value of 2.3 MPa for the von Mises stress is obtained at the acetabular cartilage just above the acetabular fossa. A progressive deformation of the femoral and acetabular cartilages can be observed as the cam deformity penetrates into the acetabulum. The nodes in the FE mesh chosen perpendicular to the axis of the subsequent flexural

Figure 4. FE mesh of the complete non-cam model.

movement present a smaller distance to the axis of rotation in the direction of the femoral neck (Figure 3(c)). This result is related to the transverse oblique orientation of the cephalic protuberance. The nodes in the mesh chosen perpendicular to the axis of the subsequent internal rotation present a progressive larger distance to the axis of rotation in the direction of the equator of the femoral head (Figure 3(d)).

For the pure flexural movement from 0° to 90°, the following results are obtained:

(1) A progressive increase in the contact pressure is observed at the femoral cartilage, initially para-equatorial, reaching a value of 8.6 MPa at 32°; as the deformity contacts the acetabular cavity, a lateral and superior migration of the zone of larger pressures can be observed; a maximum contact pressure of 13.3 MPa occurs at 90° at the most peripheral nodes near the transition zone between the neck and the femoral head on the highest elevation of the cam deformity (Figure 6(a)); also in this zone and at the end of the 90° of flexion, the maximum von Mises stress has a value of 4.6 MPa.

(2) Large contact pressures occur initially at an anterior and peripheral zone of the acetabular cartilage near the chondrolabral transition where the largest pressure has a value of 8.6 MPa at 32°; a
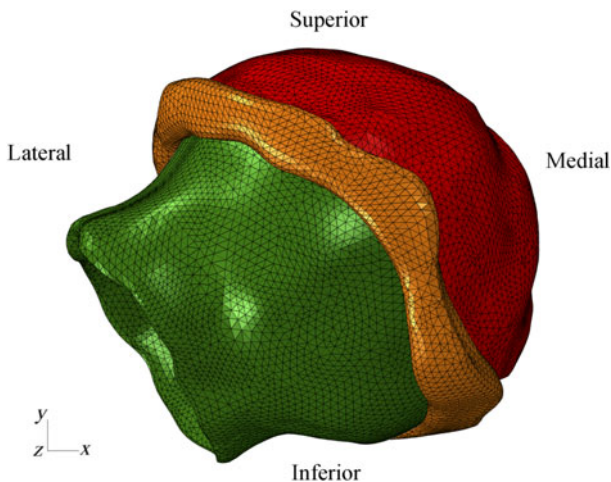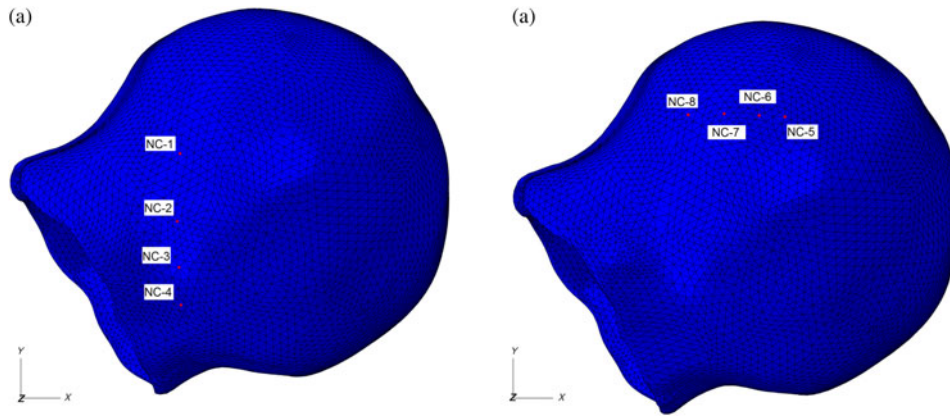
Figure 5. FE mesh of the non-cam femoral cartilage with the chosen surface nodes for (a) the pure flexion and (b) the pure internal rotation.

Table 1. Comparison between the maximum clinical angular displacements of the selected patient's right hip before surgery with those obtained with the model and the corresponding maximum contact pressures.

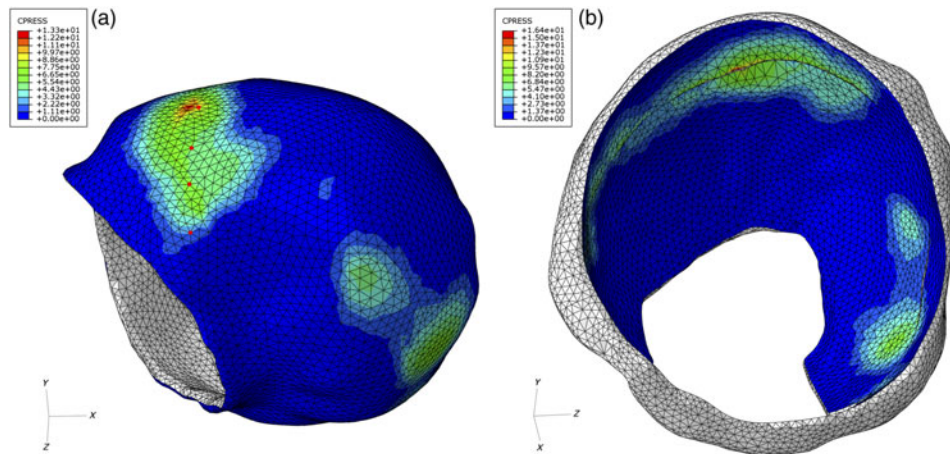|			Maximum contact pressure at the end of the movement (MPa)	
Movement	Patient	3D model	Cartilages	Labrum
Maximum pure flexion	90° (painful)	90°	12–13	16
Maxima flexion and internal rotation	90°; 0° (painful)	90°; 2.8°	13–14	16
30° of flexion and maximum internal rotation	30°; 15° (painless)	30°; 12.8°	12–13	16
Maximum pure internal rotation (in extension)	30° (painless)	24°	13–14	15

Figure 6. Contact pressures on the (a) femoral and (b) acetabular cartilages (at 90° of flexural rotation).

superior migration of this region of large pressures occurs along the periphery of the acetabular cartilage which, at 90°, is located at the superior region with a maximum value of 11.6 MPa; the maximum von Mises stress, also at 90°, occurs in the same region and has a value of 14.4 MPa; at 90° a maximum value of 16.4 MPa for the contact pressure occurs on the labrum (Figure 6(b)) and the maximum von Mises stress occurs in the same region of the labrum and has a value of 14.7 MPa.

(3) The contact pressures due to the flexural movement at the four nodes defining the line perpendicular to the axis of rotation increase with the distance of these points to the centre of
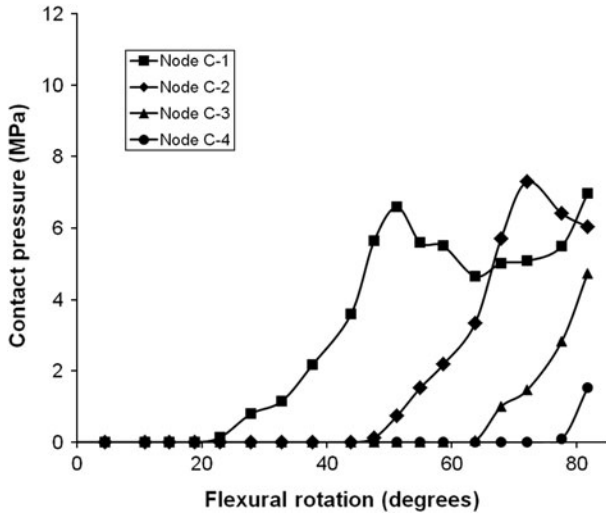
Figure 7. Contact pressure at nodes C-1, C-2, C-3 and C-4 as a function of the angular movement in the pure flexural rotation.

rotation of the head; an increase in the contact pressure occurs in all four nodes as the cam deformity penetrates into the acetabular cavity (Figure 7).

(4) Along a transversal section containing the selected four nodes it can be observed a large intrusion of the non-spherical sector which deforms substantially the acetabular and femoral cartilages in an arch of about 90°.

For the pure internal rotation from 0° to 24°, the following results are obtained:

(1) A progressive increase in the contact pressure is observed on the femoral cartilage reaching a value of 20.9 MPa at 15° at its posterior inferior region around the fovea; as the deformity contacts the acetabular cavity, the region of larger pressures moves towards the deformity; at 24°, the maximum

contact pressure is 12.8 MPa (Figure 8(a)) and a maximum von Mises stress of 5.8 MPa occurs at the posterior inferior region.

(2) At 15°, the maximum contact pressure on the acetabular cartilage has a value of 20.6 MPa at its posterior–inferior region; after that a progressive increase of the area of larger pressures is observed as well as a migration to the chondrolabral transition; at 24° of internal rotation, the maximum contact pressure has a value of 13.6 MPa on the acetabular cartilage and a value of 14.7 MPa on the labrum (Figure 8(b)); a maximum von Mises stress of 28.2 MPa occurs in a region adjacent to the acetabular fossa.

(3) The contact pressures due to the internal rotation at the four nodes defining the line perpendicular to the axis of internal rotation increase with the distance of these points to the centre of rotation of the femoral head; the contact pressure in all four nodes increases initially as the cam deformity penetrates inside the acetabular cavity; at the most peripheral nodes (nodes C-7 and C-8) a progressive increase in the contact pressure is observed; the contact pressure decreases at nodes C-5 and C-6 (closest to the equatorial region) from 12° and from 18° of rotation, respectively (Figure 9).

(4) Along a transversal section containing the selected four nodes, a smaller intrusion of the non-spherical sector into the acetabulum is observed contrary to what was found in the flexural movement.

In the case of the non-cam (normal) hip model, the contact pressures due to the flexural movement at the four nodes defining the line perpendicular to the axis of flexural rotation are shown in Figure 10 and the contact pressures due to the internal rotation at the four nodes defining the line perpendicular to the axis of internal rotation are shown in Figure 11. In both cases, the contact pressures are smaller
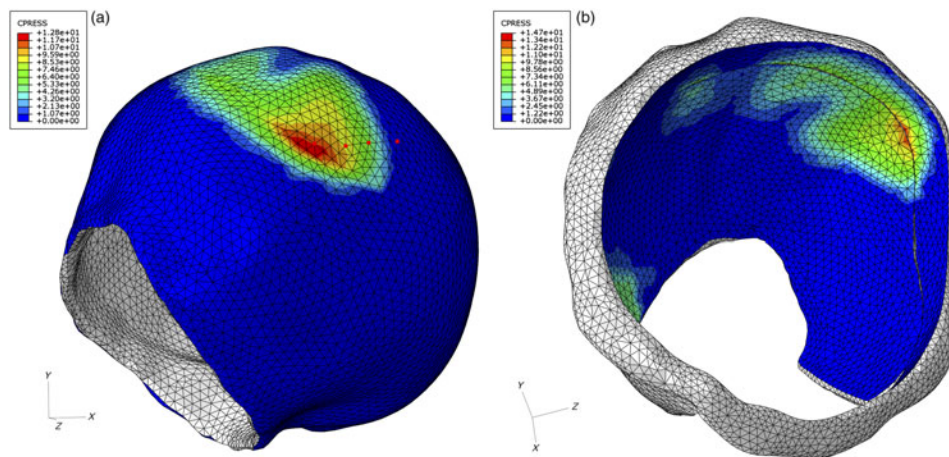

Figure 8. Contact pressures on the (a) femoral and (b) acetabular cartilages (at 24° of internal rotation).
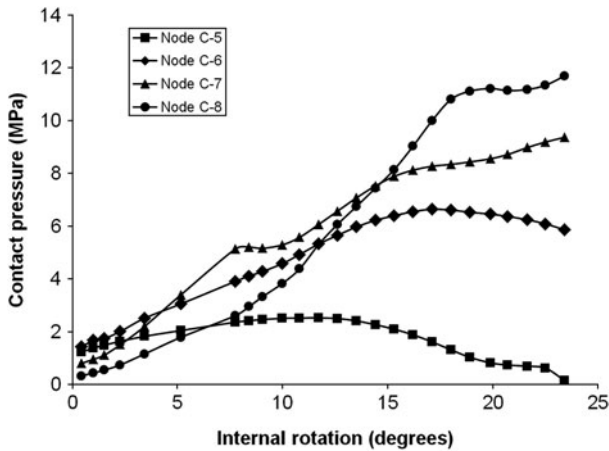
Figure 9. Contact pressure at nodes C-5, C-6, C-7 and C-8 as a function of the angular movement in the pure internal rotation.
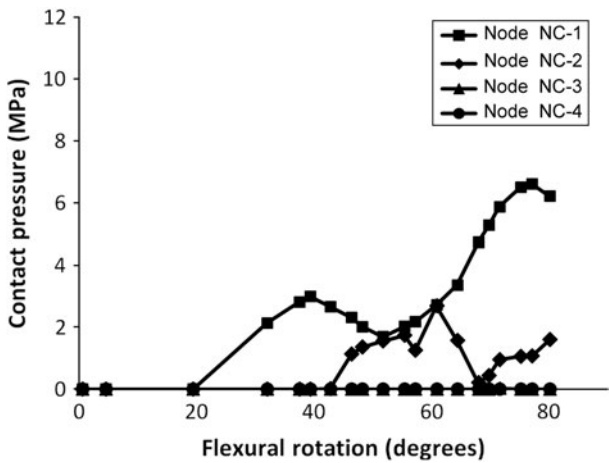

Figure 10. Contact pressure at nodes NC-1, NC-2, NC-3 and NC-4 on the non-cam model as a function of the angular movement in the pure flexural rotation.
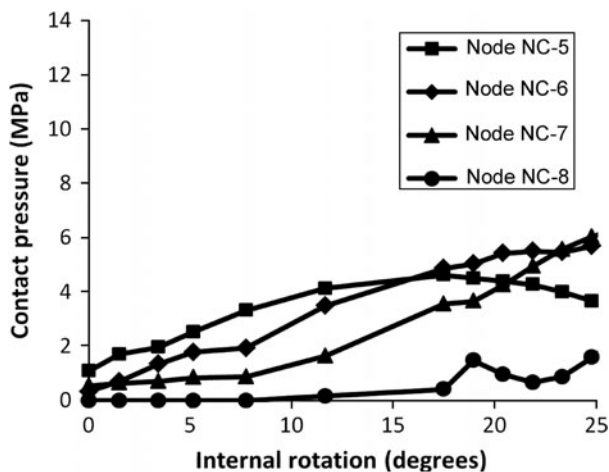

Figure 11. Contact pressure at nodes NC-5, NC-6, NC-7 and NC-8 on the non-cam model as a function of the angular movement in the pure internal rotation.

than the pressures obtained at the corresponding points in the deformity region of the cam hip. In fact maximum contact pressures of 6.60 and 6.04 MPa were obtained at the selected points of the non-cam hip during the flexural and internal rotation movements, respectively, while the corresponding contact pressures in the case of the joint with impingement were 9.65 and 11.68 MPa. It is also observed that the contact pressures obtained in the movement of internal rotation of the non-cam hip do not increase from the equator of the femoral head to the peripheral regions contrarily to what happens in the cam hip.

4. Discussion

The main objectives of our study were: (1) to contribute to a better understanding and interpretation of the mechanism of aggression of the cartilage in the cam case; (2) to build a subject-specific 3D model of the hip joint following reconstruction procedures based on medical images; (3) to perform FE analyses on this 3D model, to evaluate the order of magnitude of pressures at the contact zone and stresses in the cartilages and thus to establish a correlation with the abnormality and (4) to compare with a non-cam case and other models and clinical observations so as to validate the analyses.

The main difference between this study and other computational works (Chegini et al. 2009) resides in the fact that the FE analyses are performed on the specific anatomy of patients obtained by reconstruction methodologies and not on totally computer-generated models. In consequence, the use of more anatomically realistic models is, in our opinion, more useful and superior to other models. Each of these non-linear analyses performed on the reconstructed models requires a large amount of CPU time and careful monitoring.

The reconstruction procedures are well established, have provided invaluable models validated by orthopaedic surgeons and are ready to be used in any specific hip joint.

The major limitations of the present model are concerned with the physical behaviour of the cartilages which are so far considered linear elastic; also, although less important, the bones are considered rigid; the present model does not include other tissues present in the hip joint; finally, the manual segmentation performed on the MRA images still is of limited resolution.

Contrary to the case of the acetabular dysplasia where the maximum contact pressure occurs after the transarticular force is applied (Chegini et al. 2009), the movement seems to be the determinant factor of the genesis of high contact pressures in the case of hips with cam-type deformity.

When the non-spherical region in the transition between the neck and the femoral head is anterior, the pure flexion and/or the flexion associated with the internal rotation are the movements which produce a larger contact pressure on the articular surfaces. This mechanism of

intra-articular intrusion of the femoral cephalic protuberance is naturally dependent on its volume, on the variation of the radius of curvature of its surface and on the morphology and spatial position of the acetabulum. With the present model, elimination of the acetabular variables was sought. For this reason, a patient with a normal CE angle and with no associated retroversion was selected.

The presence of an alpha angle of 98° measured in the axial section of larger area of the cephalic asphericity in the MRA allowed the classification of the morphology as cam (Ito et al. 2001). The pure articular compression generated a maximum contact pressure of 5.2 MPa, whereas pressures of the order of 13–14 MPa were obtained in the pure flexural and internal rotation movements at the femoral/acetabular cartilages. For these movements, higher pressures occurred at the labrum (16 MPa in the flexural movement and 15 MPa in the pure rotation). These higher pressures may justify the labral damage observed in patients with FAI.

The selected movements were chosen to be the more significant in daily activities, namely standing to sitting. This movement implies flexion of the hip ranging from 60° to 90° depending on the pelvic inclination and on the mobility of the lumbar column (Heller et al. 2001; Nötzli et al. 2002). According to some authors (Ganz et al. 2003), this movement seems to be also the one that, in hips with FAI, produces the largest deformation of the acetabular cartilage and labrum as obtained in the transverse oblique sections containing the selected nodes.

The manual segmentation of the MRA images, still with limited resolution, and the extrapolation of points between the radial sections may have induced some deviation from reality. However, to ensure a 3D RBF reconstruction with lesser or attenuated artefact presence, attention is given to vector normal estimation and consistent distance-to-surface data calculations. Despite the limitations, several anatomical details are accurately reconstructed and the values obtained for the contact pressures are of the order of the values obtained with other geometrical models for similar values of the alpha and CE angles. Chegini et al. (2009) obtained, for an alpha angle of 80° and a CE angle of 30°, a value of 12.84 MPa at the acetabular cartilage in the standing to sitting movement.

At the end of both flexural and internal rotation movements, the values obtained for the maximum contact pressures on the acetabular cartilage are similar. The large pressures occurring, in the model, at 15° of internal rotation around the femoral head fovea may be explained by the absence of the round ligament. During the whole movement, the internal rotation in extension seems to produce compression in a more limited area (restricted to the chondrolabral transition; Figure 8(b)), whereas the flexural movement generates a larger and deeper contact area in the acetabulum (Figure 6(b)). These results agree with intra-operative observations (Rego et al. 2009) where

the quadrant in which the cartilage exhibits delamination and chondrolabral rupture is the antero-superior one.

The maximum clinical angular displacements of the right hip of the patient are comparable with the maximum possible amplitudes obtained with the model. The FE analyses in the cases of 90° flexion and internal rotation, 30° flexion and internal rotation and of pure internal rotation stopped at the values indicated in Table 1 due to lack of convergence. This lack of convergence is probably due to a geometrical constraint (bony anatomy): whenever there is a movement of internal rotation, the deformity tends to move in the medial direction and is not allowed to go inside the cavity because of its larger radius of curvature in the plane perpendicular to the axis of rotation (see Figure 3(d)).

In the movement of internal rotation of 24° in extension, the acetabular intrusion seems to be smaller due to the larger prominence of the deformity in the horizontal oblique plane, potentially limiting the chondral aggression to the chondrolabral transition. In the pure flexion, the intrusion is larger due to the smaller deviation of the radius of curvature in the sagittal plane, resulting in a more extensive and deeper chondral aggression in the acetabulum.

The numerical results obtained also agree with clinical and intraoperative observations (Rego et al. 2009) that patients with extensive and serious chondral acetabular lesions can present moderate cam deformities (alpha angles ranging from 55° to 70°). The fact that more central and inferior regions are spared to high compressions resulting from the movement seems to be in agreement with the observation that the isolated peripheral OA located anteriorly is associated with cam deformities (Siebenrock et al. 2003).

In both isolated movements and at the selected nodes in the FE mesh, the contact pressures increase with their distance to the centre of rotation. The nodes located in an area with larger radius of curvature of the femoral head are permanently subjected to a larger and lasting contact pressure than the nodes belonging to an area with smaller radius of curvature.

The contact pressures obtained increase from the equator of the femoral head to the peripheral regions where the radius of curvature is larger which seems to be in agreement with the macroscopic aspects (lesions) of femoral head cartilage in patients with cam-type FAI submitted to surgery (Tanzer and Noiseux 2004). At the aspherical femoral heads, submitted to a non-physiological excessive pressure, there exists systematically an aspect of increasing fibrillar chondromalacia from the equatorial region to the periphery. These observations are supported by several researchers who found, in the acetabular cartilage of patients with FAI, an increase in the expression of biological markers of OA (Wagner et al. 2003; Leunig et al. 2006).

An FE analysis of a non-cam (normal) hip was also performed for comparison with the pathological case.

In this case, the contact pressures are smaller than the pressures obtained at the corresponding points in the deformity region of the cam hip for similar rotation amplitudes. It is also observed that the contact pressures obtained in the movement of internal rotation of the non-cam hip do not increase from the equator of the femoral head to the peripheral regions contrarily to what happens in the cam hip. The corresponding FE analysis continued beyond 24°, value at which the cam case stopped as previously mentioned, suggesting that the lack of convergence observed in this last case is due to the abnormal geometry of the femoral head. Peak contact pressures of 6.60 and 6.04 MPa were obtained at the selected points of the non-cam hip during the flexural and internal rotation movements, respectively, and for an applied load of 2057 N.

Although the results of the analyses depend on a number of factors including joint incongruity, cartilage thickness and material properties, our FE models provided predictions for the contact pressures that are in the range of published experimental data on normal hip joints. Brown and Shaw (1983) reported a peak contact pressure in the hip joint of 8.8 MPa for an applied load of 2700 N. Afoke et al. (1987) measured peak contact pressures varying from 4.9 to 10.2 MPa for applied loads varying from 1980 to 2555 N and a flexural rotation of 27°. Michaeli et al. (1997) measured peak contact pressures varying from 2 to 8.4 MPa for applied loads varying from 800 to 1200 N. Also von Eisenhart et al. (1999) measured maximum contact pressures in the acetabulum during simulated walking of 6.4 ± 1.75 MPa at heel strike (for a total applied load of 94% body weight), 7.7 ± 1.95 MPa at midstance (345% body weight), 6.4 ± 1.33 MPa at heel-off (223% body weight) and 5.4 ± 1.7 MPa at toe-off (80% body weight). Finally, Anderson et al. (2008) reported experimental pressures ranging from 1.7 to 10.0 MPa during simulated walking, stair climbing and descending stairs.

No experimental reported contact pressures in joints with impingement were found with which our results could be compared. However, computationally, Chegini et al. (2009) obtained on a virtual pathological hip joint a value of 12.84 MPa for the pressure at the acetabular cartilage in the standing to sitting movement, value that is in the range shown in Table 1 for the maximum contact pressure at the end of the performed movements.

The main conclusion of this work is that the movement is the determinant factor for the occurrence of high contact pressures in hips with cam deformities. In fact high pressures were obtained at the labrum in both movements which may justify the damage observed in patients with this pathology. Also in the flexural movement an increase in the contact pressure from the para-equatorial region towards the deformity was observed in the femoral cartilage while larger pressures occur in the antero-superior quadrant of the acetabulum. In the internal

rotation case, a similar increase in the contact pressures was observed in the femoral cartilage while larger pressures occur in the superior region of the acetabulum near the chondrolabral transition. These observations reinforce the proposed mechanism of cartilage damage in the cam-type FAI and the macroscopic changes that are intra-operatively routinely found at the femoral head in these patients. Finally, this model, closer to anatomical reality than others, may be understood as a rational explanation for a mechanism that may induce degeneration of the cartilage due to high contact pressures and can, therefore, be considered an '*in vivo*' model of human OA.

Although the model has the limitations mentioned before, the overlap between the clinical observations and the results obtained from the FE analyses brings some optimism to future developments in this area. These may include the consideration of the cartilages as porous materials; also, improvements in the reconstruction namely the resolution of the manual segmentation by obtaining a larger number of MRA images in order to avoid the need for excessive extrapolations; reconstruction of hip joints including other surrounding tissues like ligaments; consideration of bones as non-rigid; consideration of other imposed forces, movements and more complex boundary conditions.

Acknowledgements

References

Afoke NYP, Byers PD, Hutton WC. 1987. Contact pressures in the human hip joint. J Bone Joint Surg Br. 69:536–541.

Anderson AE, Ellis BJ, Maas SA, Peters CL, Weiss JA. 2008. Validation of finite element predictions of cartilage contact pressure in the human hip joint. J Biomech Eng. 130:051008.

Bachtar F, Chen X, Hisada T. 2006. Finite element contact analysis of the hip joint. Med Biol Eng Comput. 44:643–651.

Beck M, Leunig M, Parvizi J, Boutier V, Wyss D, Ganz R. 2004. Anterior femoroacetabular impingement: part II. Midterm results of surgical treatment. Clin Orthop Relat Res. 418:67–73.

Bergmann G, Deuretzbacher G, Heller M, Graichen F, Rohlmann A, Strauss J, Duda GN. 2001. Hip contact forces and gait patterns from routine activities. J Biomech. 34:859–871.

Brown TD, Shaw DT. 1983. *In vitro* contact stress distributions in the natural human hip. J Biomech. 16:373–384.

Carr JC, Beatson RK, Cherrie JB, Fright WR, McCallum BC, Evans TR. 2001. Reconstruction and representation of 3D objects with radial basis functions. Paper presented at: SIGGRAPH '01. Proceedings of the 28th Annual International Conference on Computer Graphics and Interactive Techniques, New York, USA.

Carr JC, Fright WR, Beatson RK. 1997. Surface interpolation with radial basis functions for medical imaging. IEEE Trans Med Imaging. 16:96–107.

Chegini S, Beck M, Ferguson SJ. 2009. The effects of impingement and dysplasia on stress distributions in the hip joint during sitting and walking: a finite element analysis. J Orthop Res. 27:195–201.

Clohisy JC, McClure JT. 2005. Treatment of anterior femoroacetabular impingement with combined hip arthroscopy and limited anterior decompression. Iowa Orthop J. 25:164–171.

Ganz R, Parvizi J, Beck M, Leunig M, Nötzli HP, Siebenrock KA. 2003. Femoroacetabular impingement: a cause for osteoarthritis of the hip. Clin Orthop Relat Res. 417:112–120.

Genda E, Iwasaki N, Li G, MacWilliams BA, Barrance PJ, Chao EYS. 2001. Normal hip joint contact pressure distribution in single-leg standing – effect of gender and anatomic parameters. J Biomech. 34:895–905.

Heller MO, Bergmann G, Deuretzbacher G, Dürselen L, Pohl M, Claes L, Haas NP, Duda GN. 2001. Musculo-skeletal loading conditions at the hip during walking and stair climbing. J Biomech. 34:883–893.

Hodge WA, Fijan RS, Carlson KL, Burgess RG, Harris WH, Mann RW. 1986. Contact pressures in the human hip joint measured *in vivo*. Proc Natl Acad Sci USA. 83:2879–2883.

Ito K, Minka MA, II, Leunig M, Werlen S, Ganz R. 2001. Femoroacetabular impingement and the cam-effect. A MRI-based quantitative anatomical study of the femoral head-neck offset. J Bone Joint Surg Br. 83:171–176.

Jorge JP, Simões FMF, Pires EB, Lopes DS, Rego PA. 2010. Finite element studies of a hip joint with femoroacetabular impingement of the cam type. Paper presented at: CMBBE 2010. Proceedings of the 9th International Symposium Computer Methods in Biomechanics and Biomedical Engineering, Valencia, Spain.

Leunig M, Beck M, Dora C, Ganz R. 2006. Femoroacetabular impingement: trigger for the development of coxarthrosis. Orthopade. 35:77–84.

Lopes DS, Jorge JP, Pires EB, Simões FMF, Rego PA. 2010. A three dimensional geometric model of a hip joint presenting a femoral head deformity based on radial magnetic resonance arthrography images. Computational vision and medical image processing. London: Taylor & Francis Group. p. 105–110.

Lopes DS, Simões FMF, Pires EB, Rego PA. 2009. Modelação Biomecânica do Conflito Femuro-Acetabular do Tipo Cam. Paper presented at: 3rd Biomechanics National Congress. Proceedings of the 3rd Biomechanics National Congress, Bragança, Portugal.

Macirowski T, Tepic S, Mann RW. 1994. Cartilage stresses in the human hip joint. J Biomech Eng. 116:10–18.

Michaeli DA, Murphy SB, Hipp JA. 1997. Comparison of predicted and measured contact pressures in normal and dysplastic hips. Med Eng Phys. 19:180–186.

Nötzli HP, Wyss TF, Stoecklin CH, Schmid MR, Treiber K, Hodler J. 2002. The contour of the femoral head-neck junction as a predictor for the risk of anterior impingement. J Bone Joint Surg Br. 84:556–560.

Rego P, Costa J, Lopes G, Monteiro J. 2009. Surgical hip dislocation, the Portuguese experience. Personal communication. 10th EFORT Congress, Vienna, Austria.

Shepherd DET, Seedhom BB. 1997. A technique for measuring the compressive modulus of articular cartilage under physiological loading rates with preliminary results. Proc Inst Mech Eng H. 211:155–165.

Siebenrock KA, Schoeniger R, Ganz R. 2003. Anterior femoro-acetabular impingement due to acetabular retroversion. Treatment with periacetabular osteotomy. J Bone Joint Surg Am. 85:278–286.

Tanzer M, Noiseux N. 2004. Osseous abnormalities and early osteoarthritis: the role of hip impingement. Clin Orthop Relat Res. 429:170–177.

Teodoro P, Pires P, Martins J, Sá da Costa J. 2009. Proximal femur parameterization and contact modeling for hip resurfacing surgery. Paper presented at: 3rd Biomechanics National Congress. Proceedings of the 3rd Biomechanics National Congress, Bragança, Portugal.

von Eisenhart R, Adam C, Steinlechner M, Müller-Gerbl M, Eckstein F. 1999. Quantitative determination of joint incongruity and pressure distribution during simulated gait and cartilage thickness in the human hip joint. J Orthop Res. 17:532–539.

Wagner S, Hofstetter W, Chiquet M, Mainil-Varlet P, Stauffer E, Ganz R, Siebenrock KA. 2003. Early osteoarthritic changes of human femoral head cartilage subsequent to femoro-acetabular impingement. Osteoarthritis & Cartilage. 11:508–518.

Yoshida H, Faust A, Wilckens J, Kitagawa M, Fetto J, Chao EY-S. 2006. Three-dimensional dynamic hip contact area and pressure distribution during activities of daily living. J Biomech. 39:1996–2004.